J Solid State Electrochem (2008) 12:421–435
DOI 10.1007/s10008-007-0402-5

ORIGINAL PAPER

Electrochemical and spectral properties of some tantalocene derivatives with one pentamethylated cyclopentadienyl ligand: $Cp^*(Cp\text{-}R)TaCl_2$, R = H, $SiMe_3$ or $(CH_2)_3NC_4H_4$

Mikhail A. Vorotyntsev · Magdalena Skompska · Magdalena Graczyk · Jürgen Heinze · Jerome Goux · Pierre Le Gendre · Claude Moise

Received: 24 January 2007 / Revised: 6 May 2007 / Accepted: 31 May 2007 / Published online: 21 September 2007

Abstract Three tantalocene dichloride complexes, $Cp^*(Cp\text{-}R)Ta(IV)Cl_2$, with one pentamethylated cyclopentadienyl ligand, $Cp^* = \eta^5\text{–}C_5Me_5$, Me = CH_3, and one monosubstituted cyclopentadienyl ligand, Cp-R, Cp = $\eta^5\text{–}C_5H_5$, R = H, $SiMe_3$ or $(CH_2)_3NC_4H_4$, have been studied in acetonitrile solutions with cyclic voltammetry in the ranges of the Ta(IV) oxidation to Ta(V) or of its reduction to Ta(III). The former transition is reversible, while the latter one gives an irreversible wave due to the dissociation of the reduced complex with the loss of one chloride ligand. The redox transformation from the initial state of complex $Cp^*CpSiMe_3TaCl_2$ to its oxidized state, $Cp^*CpSiMe_3TaCl_2^+$, and back was monitored by spectroelectrochemical measurements in a thin-layer acetonitrile solution. Kinetic data for the evolution of the UV-visible spectrum of the system in the course of the double potential step experiment were treated on the basis of two theoretical models as the reactant diffusion across the solution layer without or with taking into account ohmic losses. The values of the diffusion coefficients of the complex in its initial and oxidized (cationic) states have been estimated. It was demonstrated that this complex in each of two oxidation states, Ta(IV) or Ta(V), is represented by a single molecular form. An attempt to deposit a conducting polymer film by oxidation of the tantalocene complex containing a pyrrole group attached to the Cp ring, $Cp^*Cp(CH_2)_3PyTaCl_2$, led to a thin insulating layer at the electrode surface because of an inhibiting effect of chloride anions.

Keywords Tantalum · Metallocene · Pentamethylated tantalocene complexes · UV-visible spectra · Spectroelectrochemistry · Redox transition · Thin layer voltammetry and chronoamperometry · Diffusion coefficient · Ohmic potential drop

Abbreviations

AN	acetonitrile
THF	tetrahydrofuran
DCM	dichloromethane
$TBAPF_6$	tetrabutylammonium hexafluorophosphate $(C_4H_9)_4NPF_6$
Cp	cyclopentadienyl ligand, $\eta^5\text{–}C_5H_5$
Cp*	pentamethylated cyclopentadienyl ligand, $\eta^5\text{–}C_5Me_5$, Me = CH_3
$Cp^*CpTaCl_2$	tantalocene dichloride complexes: $(\eta^5\text{–}C_5Me_5)$ $(\eta^5\text{–}C_5H_5)TaCl_2$
$Cp^*CpSiMe_3TaCl_2$	$(\eta^5\text{–}C_5Me_5)$ $(\eta^5\text{–}C_5H_4SiMe_3)TaCl_2$
$Cp^*(Cp(CH_2)_3Py)TaCl_2$	$(\eta^5\text{–}C_5Me_5)$ $(\eta^5\text{–}C_5H_4(CH_2)_3NC_4H_4)TaCl_2$

Dedicated to Professor Oleg Petrii on the occasion of his 70th birthday on August 24th, 2007.

M. A. Vorotyntsev (✉) · M. Graczyk · J. Goux · P. Le Gendre · C. Moise
ICMUB–UMR 5260 CNRS, University of Bourgogne,
Bat. Mirande, 9 avenue A. Savary, BP 47 870,
21078 Dijon Cedex, France
e-mail: mv@u-bourgogne.fr

M. Skompska
Department of Chemistry, Warsaw University,
ul. Pasteura 1,
02 093 Warsaw, Poland

J. Heinze
Inst. Physik. Chemie, Albert-Ludwigs-Universität Freiburg,
Albertstrasse, 21,
79104 Freiburg, Germany

Introduction

Bis(cyclopentadienyl) complexes of transition metals (metallocenes) employed as single-electron transferring species are important reagents in organic synthesis [1–10]. The most extensive studies have been devoted to Ti and Zr complexes as well as their derivatives, while less attention has been paid to analogous complexes of other "early transition metals". Initial studies of bis(pentamethylcyclopentadienyl) complexes of heavier Group 5 elements, niobium and tantalum, were performed in early 80th [11–13], followed by the development of efficient synthetic routes to their dichloride complexes [14, 15]. Tantalocene derivatives represent a promising group of products from the point of view of their possible applications in organic catalysis, e.g., in olefin polymerization [16–19] and in CH-bond activation [20, 21].

Electrochemical properties of solute metallocene complexes of early transition metals (Groups 4–6) have been studied in numerous publications, the principal attention having been paid to titanocene dichloride, Cp_2TiCl_2, and its derivatives, owing to their high stability. Much less has been done in electrochemistry of tantalocene complexes where the only studied system was a formal analog of Cp_2TiCl_2, a dichloride complex of tantalum(IV), Cp_2TaCl_2 [22, 23].

Despite the similarity of their chemical formulas, these complexes of Ti and Ta demonstrate quite different properties, as Ti(IV) represents a d^0 electronic state while Ta(IV) is in the d^1 state. The presence of this d-electron makes Ta(IV) complexes very sensitive to oxygen and moisture, with their easy oxidation to Ta(V). These properties result in the necessity to synthesize, keep, and characterize them under a strictly controlled argon atmosphere.

In our actual work, we were interested in extending these studies of Cp_2TaCl_2 to characterize three derivatives of this complex, Cp*(Cp-R)$TaCl_2$, in which one of the Cp ligands was pentamethylated (Cp*) while another Cp ring was either intact or modified by a substituting group, Cp-R, R= $SiMe_3$ (**1**) or $(CH_2)_3NC_4H_4$ (**2**) (the latter complex was synthesized for the first time). Two complementary techniques have been applied, cyclic voltammetry and spectroelectrochemistry, in the UV-visible range.

The electrochemical method was used to study the transformation of these three complexes of Ta(IV) to those of Ta(V) or Ta(III). The spectroscopic measurements were realized for one of these complexes, Cp*Cp$SiMe_3TaCl_2$, inside a thin solution layer between the electrode and the wall. This construction allowed us to study the mechanism of the redox transformations of this complex, Ta(IV)–Ta(V)–Ta(IV), induced by the double potential step, in particular, to check whether the complex in its oxidized state, Ta(V), is represented by a single or several molecular forms.

To estimate the diffusion coefficients of the initial and oxidized forms of this complex, the temporal evolution of the spectrum was analyzed with the use of two models, one of them considering the process as purely diffusional, while another model took also into account the ohmic potential drop between working and reference electrodes.

Another aim of this work was an attempt to immobilize this tantalocene dichloride complex inside a conducting polymer matrix. We used the same strategy which had been successfully applied for immobilization of the titanocene dichloride complex inside a conducting polymer film with the polypyrrole [24, 25] or PEDOT [26] matrices. To achieve this goal, one (non-methylated) of the Cp ligands of the tantalocene complex was linked to nitrogen of pyrrole. A successful polymerization of this pyrrole moiety would allow us to immobilize the tantalocene dichloride complex inside a conducting polymer film, with potential applications of such system in heterogeneous catalysis of organic and polymerization reactions. Preliminary tests of reactions of solute reactants at the electrodes modified with titanocene dichloride containing films have been initiated recently [27–29].

Experimental

Synthesis of tantalocene complexes

Reactions were carried out under inert atmosphere using Schlenk techniques (argon). Solvents were dried and distilled under argon. $(C_5H_4(CH_2)_3NC_4H_4)^-$ Li^+, Cp*$TaCl_4$, and Cp*Cp$TaCl_2$ were prepared according to literature methods [24, 30].

The purity of Cp*Cp$TaCl_2$ used for this study was controlled by elemental analysis performed with EA 1108 CHNS-O FISONS instrument: Anal. Calc. for $C_{15}H_{20}TaCl_2$: C, 39.84; H, 4.46. Found: C, 40.10; H, 4.85.

Nuclear magnetic resonance technique was not used for characterization of Ta(IV) complexes in Fig. 1 because of their paramagnetic nature (d^1 complexes).

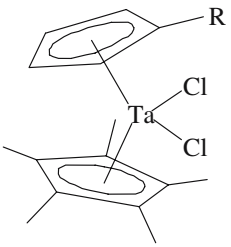

R = H

R = $SiMe_3$ **1**

R = $(CH_2)_3NC_4H_4$ **2**

Fig. 1 Structure of tantalocene complexes studied in this paper: R = H or $SiMe_3$ (**1**) or $(CH_2)_3NC_4H_4$ (**2**)

Synthesis of tantalum complex(η^5–C_5Me_5)(η^5–$C_5H_4SiMe_3$)$TaCl_2$ (***Cp*CpSiMe$_3$TaCl$_2$***) (***1***)

Complex **1** was prepared according to the literature method [31] using rigorously dried solvents and under dry inert atmosphere. The complex is a dark green solid soluble in aromatic and saturated hydrocarbons, ethyl ether, and acetonitrile. Anal. Calc. for $C_{18}H_{28}SiTaCl_2$: C, 41.23; H, 5.38. Found: C, 41.10; H, 5.05. Its further characterization and reactivity have been described in detail elsewhere [31, 32].

Synthesis of complex (η^5–C_5Me_5)(η^5–$C_5H_4(CH_2)_3NC_4H_4$)$TaCl_2$ (***Cp*(Cp(CH$_2$)$_3$Py)TaCl$_2$***) (***2***)

Compound **2** was synthesized according to Bercaw's method [30] reported for (η^5–Cp*)(η^5–C_5H_5)$TaCl_2$ with minor modifications.

Cp*$TaCl_4$ [4.58 g (10 mmol)] was reduced with 0.5 equiv. of Mg in THF in the presence of 1 equiv. of PMe_3. Removal of the solvent led to a red residue. This crude product was treated with 1.80 g (10 mmol) $(C_5H_4(CH_2)_3NC_4H_4)^-$ Li^+ in toluene at 100 °C. After 12 h of stirring, extraction in toluene afford the green paramagnetic product **2** in a nearly quantitative yield (86%).

Anal. Calc. for $C_{22}H_{29}TaCl_2N$: C, 47.23; H, 5.23; N, 2.50. Found: C, 46.61; H, 5.23; N, 2.8.

The ESR spectrum in toluene showed an eight-line spectrum: a_{iso}=113.98 G ; g_{iso}=1.9293; H_0^{iso}=3569.697 G; H_{DPPH}=3437.375; g_{DPPH}=2.0036.

Other chemicals and preparation of solutions

The studied Ta(IV) complexes (Fig. 1), Cp*CpTaCl$_2$, Cp*CpSiMe$_3$TaCl$_2$, and Cp*(Cp(CH$_2$)$_3$Py)TaCl$_2$ are very sensitive even to traces of oxygen. Therefore, their solutions were prepared under argon atmosphere using deoxygenated solvents containing 0.1 M $TBAPF_6$ as the supporting electrolyte.

Electrochemical and spectroelectrochemical experiments

All electrochemical studies were realized in a conventional one-compartment cell with a platinum wire counter electrode (CE) and Ag/(0.01 M $AgNO_3$+0.1 M $TBAPF_6$ in CH_3CN) double junction (with 0.1 M $TBAPF_6$ in AN between two frits) reference electrode (RE).

All potentials in the text (if not specified otherwise) are given vs this RE. Its potential is about 0.32 V vs SCE (aq) if both electrodes are immersed into AN solution and about 0.33 V for THF solution [24].

All solutions were deoxygenated using vacuum technique. Experiments were performed under dry and oxygen-free argon atmosphere. For deposition experiments, acetonitrile (AN, Carlo Erba HPLC grade) was used as received. For all other experiments, AN was refluxed over CaH_2 (Aldrich) for 12 h then distilled and kept after it over molecular sieves 4 Å (Aldrich). THF (Acros Organics stabilized by hydroquinone) was distilled over metallic sodium and benzophenon (Merck) before use. $TBAPF_6$ (Aldrich, electrochemical grade) was stored at 80 °C and dried under vacuum at 80 °C for 2 h before use.

UV-visible spectra of a thin solution layer between the quartz cell bottom and a mirror-like reflecting Pt working electrode (WE) were measured using external optical fiber bundle (Laber, Rüsselsheim, Germany) placed perpendicular to WE surface [33]. A distance between working electrode and flat quartz bottom of the cell could be changed within the range from 10 μm to 10 mm (the value of the layer thickness in real experiments could not be controlled precisely, see below). A platinum wire was used as counter electrode, and a silver wire was used as reference electrode. Potential of Ag wire vs the above double junction Ag/0.01 M $AgNO_3$ + AN electrode was −0.37 V.

The spectra were registered by means of spectrophotometer ZEISS MCS 500 including power supply NMC 105, lamp cassette CLH 500, spectrometer cassette MCS 521 Vis, fiber optics with the spectral window from 380 nm to 1,100 nm. This device allows to register spectra with a great speed (up to 1 ms for each well-resolved spectrum). The baseline correction was carried out with the empty cell and the electrode at the distance of 80 μm from the bottom. Spectra of the respective reagent-free solvent–electrolyte system were recorded separately and subtracted from the original spectrum. After each experiment under thin layer conditions, the electrode was lifted and the solution was stirred. The electrochemical measurements were performed by means of Jaissle potentiostat-galvanostat IMP 88 and PAR 175 programmer. Data were recorded with Philips Model PM 8 13 1 X-Y recorder.

Results and discussion

Electrochemical behavior of Cp*CpSiMe$_3$TaCl$_2$ and Cp*CpTaCl$_2$ in AN and THF solutions

In the oxygen-free conditions, these complexes of Ta(IV) are redox-inactive in AN and THF solutions within the potential range about −0.7 to −1.5 V. The extension of the potential scan in the positive or negative direction leads to the oxidation or reduction of these species. As a typical example, Fig. 2 presents cyclic voltammograms of Cp*CpSiMe$_3$TaCl$_2$ in 0.1 M $TBAPF_6$ acetonitrile solution on Pt electrode.

A pair of oxidation and reduction peaks (A and A′) is observed at the potentials −0.55 and −0.64 V, respectively.

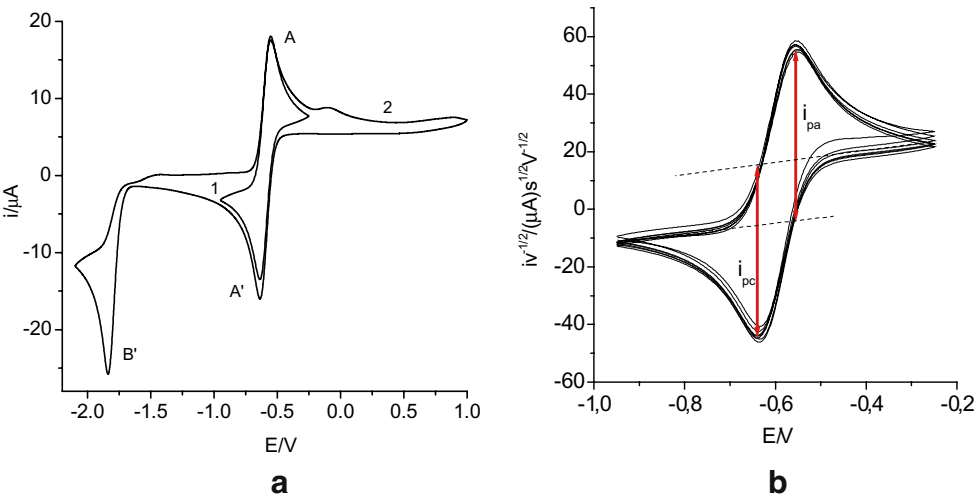

Fig. 2 **a** Cyclic voltammograms of $Cp^*CpSiMe_3TaCl_2$ in AN + 0.1 M $TBAPF_6$ in different potential ranges: −0.9 V→−0.3 V→−0.9 V (curve 1) and −0.9 V→1.0 V→−2.1 V→−0.9 V (curve 2). Reactant concentration about 8 mM (not controlled precisely due to the solvent evaporation because of a strong flow of very dry Ar). Pt electrode. Scan rate 100 mV/s. **b** Comparison of "normalized" voltammograms (stabilized response: third cycle for each scan rate), i.e., $i/v^{1/2}$ vs E curves for different scan rates in the range 40–300 mV/s

The position of both peaks does not change in the multicycle experiment. Diffusion character of the process is indicated by the characteristic shape of voltammogram, the difference between the peak potentials (90 mV), the independence of the peak potentials on the scan rate and by the equality of the corrected anodic and cathodic peak current, $i_{pa}^* = i_{pc}^*$ (the way of their determination is shown in Fig. 2b). A more quantitative proof is given in Fig. 2b: coincidence of "normalized voltammograms" for different scan rates, in the range 40–300 mV/s, obtained by division of the current by the value of $v^{1/2}$.

The same pair of reversible peaks has been observed for $Cp^*CpSiMe_3TaCl_2$ in THF as well as for $Cp^*CpTaCl_2$ in AN and THF; see the peak potential values in Table 1. In both solvents, the substitution with $SiMe_3$ leads to a small negative shift of the peaks related probably to slight electron-donor properties of this group. The comparison of the data for Cp_2TaCl_2 and its pentamethylated analog, $Cp^*CpTaCl_2$, confirms a well-known electron donating property of alkyl groups [22, 34], resulting in a higher electron density at the metal and corresponding to a negative shift of the redox potentials. One can compare this effect to that observed for an analogous titanocene dichloride complex where the full methylation of both Cp rings, $Cp^*_2TiCl_2$, led to about 200-mV shift (but in a different solvent, dichloromethane) [34, 35] while the attachment of a single substituent in one of the Cp rings, $Cp(Cp(CH_2)_3Py)TiCl_2$ gave only a small shift, about 30–40 mV [22].

To establish the molecular mechanism of this transformation, Ta(IV)→Ta (V), complex (**1**) was oxidized chemically by $(Cp_2Fe)^+PF_6^-$ in THF (the procedure is described in [36]) to obtain a cationic derivative, $(Cp^*CpSiMe_3TaCl_2)^+PF_6^-$. The CV of its solution shows a pair of

Table 1 Peak potentials of tantalocene dichloride complexes Comment: The data for Cp_2TaCl_2 were obtained by recalculation of the values given in [23] for THF and in [22] for DCM, the difference between our RE and aqueous SCE being taken as 0.33 V if both electrodes are immersed into a THF solution and as 0.22 V into DCM [24]

Complex	Solvent	E_{pc} (V) vs Ag/Ag^+	E_{pa} (V) vs Ag/Ag^+	ΔE_p (mV)
Cp_2TaCl_2	THF	−0.48	−0.42	60
		−1.80		
	DCM	−0.37	−0.29	80
		−1.82		
$Cp^*CpTaCl_2$	THF	−0.51	−0.44	70
		−1.90		
	AN	−0.59	−0.48	110
		−1.81		
$Cp^*CpSiMe_3TaCl_2$	THF	−0.56	−0.46	100
		−1.83		
	AN	−0.64	−0.55	90
		−1.83		
$Cp^*(Cp(CH_2)_3Py)TaCl_2$	AN	−0.62	−0.53	90
		−1.90	1.09	

reversible reduction–reoxidation peaks at the same potentials as the oxidation–reduction peak potentials for $Cp^*CpSiMe_3TaCl_2$ (Fig. 3).

It allowed us to conclude that the electron transfer process could be described by the simple mechanism:

$$Cp^*(Cp-R)\,Ta^{IV}\,Cl_2 - e^- \rightleftharpoons \left[Cp^*(Cp-R)\,Ta^{V}Cl_2\right]^+ \quad (1)$$

where R=H, $SiMe_3$. This conclusion is in conformity with a similar mechanism proposed for a non-derivatized complex, Cp_2TaCl_2 [22, 23].

In AN or THF solutions of Ta(IV) complexes, the potential scan towards more negative potentials leads to their reduction up to Ta(III), e.g., at −1.83 V (peak B′ in Fig. 2a) for $Cp^*CpSiMe_3TaCl_2$ in AN; see the peak potential values for other complexes/solvent in Table 1. The voltammetric wave is practically irreversible without a noticeable reoxidation wave.

The mechanism of this step has been analyzed in [23] for the non-derivatized complex, Cp_2TaCl_2, in THF. It was concluded that the electron transfer gave an anionic complex, $Cp_2TaCl_2^-$, which was subject to a dissociation step with the loss of one of the chloride ligands by the complex, $Cp_2TaCl+Cl^-$. The equilibrium of this step was strongly temperature dependent, being shifted in favor of the anion radical for lower temperatures leading to the voltammogram of a reversible type [23]. On the contrary, for the room temperature or at addition of AN into THF, the dissociation degree increased strongly, and it resulted in the voltammogram of an irreversible type [23]. At a bit longer timescale, the generated tantalocene monochloride gave a mixed valence complex, Ta(III)–Ta(IV), with the initial form, Cp_2TaCl_2, but this reaction did not manifest itself at the time scale of the voltammogram [23].

A similar conclusion on the mechanism of this reduction step for the same non-derivatized complex in dichloromethane was derived in [22].

The practically irreversible character of the CV wave at −1.83 V in Fig. 2a, as well as the identical heights of both cathodic waves, led us to the conclusion that in this system (our data correspond to room temperature), the chloride loss is sufficiently rapid and almost complete (to ensure the irreversibility of the wave), while the formation of the mixed complex is too slow to influence the shape of the voltammogram (its height would be lowered, up to two times, compared to the first cathodic wave if the mixed valency complex were formed rapidly). It corresponds to the mechanism:

$$Cp^*(Cp-R)\,Ta^{IV}\,Cl_2 + e^- \rightleftharpoons Cp^*(Cp-R)\,Ta^{III}\,Cl_2^- \rightleftharpoons Cp^*(Cp-R)\,Ta^{III}\,Cl + Cl^-,\ R = H, SiMe_3 \quad (2)$$

Most probably, the chloride loss is accompanied by the parallel insertion of another ligand, e.g., a solvent molecule, or by the dimerization step giving a Ta(III)–Ta(III) complex, in analogy with the reduction of titanocene dichloride and other similar complexes [22, 23, 37, 38].

Spectroelectrochemical behavior of $Cp^*CpSiMe_3TaCl_2$ in acetonitrile solution

Spectroelectrochemical experiments were carried out in the solution of 15 mM $Cp^*CpSiMe_3TaCl_2$ in AN in the range of the reversible transformation: Ta(IV)→Ta(V)→Ta(IV). The

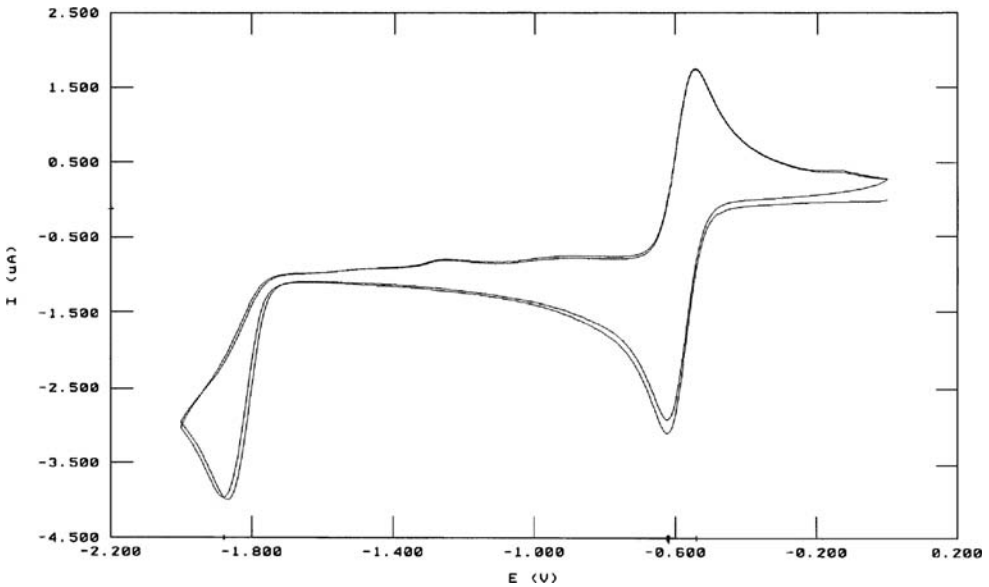

Fig. 3 Cyclic voltammogram on Pt electrode in $(Cp^*(CpSiMe_3)TaCl_2)^+PF_6^-$ + 0.1 M $TBAPF_6$/AN at the scan rate 100 mV/s

construction of the system in which the beam crossed twice a thin solution layer allowed us to perform "electrolysis" of this portion of solution, i.e., to transform practically all complexes inside this small volume from their initial state, Ta(IV), to the oxidized one, Ta(V), and then back to Ta(IV).

The cyclic voltammogram recorded in this spectroelectrochemical cell at the scan rate of 100 mV/s has got a shape typical for a diffusion-controlled redox process, i.e., it is similar to that obtained in the conventional cell (Fig. 2a, curve 1). The reason of this analogy is a very small thickness of the non-stationary diffusion layer for this scan rate, about 30–50 μm (for the diffusion coefficients in the range of $1–3\times10^{-5}$ cm^2/s expected for tantalocene complexes). In our experiments, the physical thickness of the solution layer between the cell's wall and the mirror Pt electrode is much greater, i.e., the transport conditions are practically equivalent to the semi-infinite system. As a consequence, only a small fraction of the reactant inside this solution layer is transformed during the potential scan. A larger separation between the peaks in Fig. 4a (compared to that in Fig. 2b) is due to a greater WE-RE electric resistance in this thin-layer configuration of the spectroelectrochemical cell (in which RE is located in the bulk solution, far away from WE inside the thin solution layer), a larger electrode surface and a higher concentration of the complex (leading to higher currents).

An optimum distance between the electrode and the cell bottom was chosen to maintain a sufficiently high absorbance of the solution layer (but within the range of the linear response of the spectrophotometer, well below 1) and, on the other hand, to approach the thin layer conditions. The chosen distance, crudely estimated as about 100–200 μm, does not correspond to ideal "thin layer voltammetry" conditions as may be seen in Fig. 4b: The current does not vanish outside the voltammetric peaks due to a supply of additional portions of the reactant to the layer from the outside solution; the peak potentials for anodic and cathodic processes are not identical because of an extended diffusion time across the layer (several tens of second) and the ohmic potential drop. However, this distance was still sufficiently small to minimize the effect of the exchange between the layer and the outside solution within the time scale of redox experiments.

Spectroelectrochemical experiments were performed either with a slow sweep of the potential (1 mV/s) in both directions (Fig. 4b) or as a double step between two potential values corresponding to the initial, Ta(IV), and final, Ta(V), states of the complex. The evolution of the spectrum of the complex in the course of its oxidation and the subsequent re-reduction was identical for both regimes. A detailed analysis below will be based on the potential-step data, as they allow an easier theoretical treatment.

The AN solution of complex $Cp^*CpSiMe_3TaCl_2$ in its initial (neutral) state has got a green color. Its spectrum (curve 1 in Fig. 5) represents a combination of the absorption band near 670 nm and a tail in the blue part of the visible range related to a strong absorption in the UV range (not shown in Fig. 5 because of measuring device limitations).

The complex is both oxidation states belongs to "bent metallocenes" in which their four ligands form a distorted tetrahedron so that the planes of two cyclopentadienyl rings are not parallel. A general theory of the electronic structure (orbitals and energy levels) for this class of molecules was proposed in [39] on the basis of a qualitative reasoning. Further quantum-chemical calculations (e.g., [40] for Cp_2TiCl_2) confirmed its predictions, although the calculated distances between the electronic energy levels corresponding to the electronic transitions in the course of the light absorption do not match well to the observed optical energy bands of the complex.

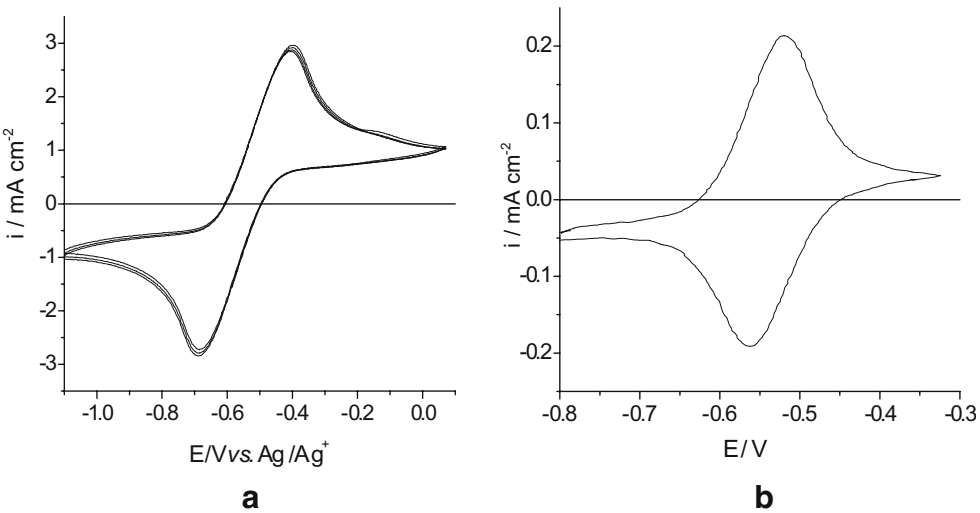

Fig. 4 Cyclic voltammograms of $Cp^*CpSiMe_3TaCl_2$ recorded in the spectroelectrochemical cell at the scan rate 100 mV/s (**a**) and 1 mV/s (**b**)

As such a detailed analysis for tantalocene dichloride complexes is not available, we will have to base this discussion on the analogy of our complex with the titanocene dichloride which was studied more extensively. As the Ta atom has an extra d-electron compared to Ti, one should expect a similarity between the complexes of Ta(V) and Ti(IV) or between those of Ta(IV) and Ti(III).

In conformity with these expectations, solutions of both former complexes, Ta(V) and Ti(IV), are transparent in the most of the visible range, above 600 nm (including the adjacent NIR range), while a strong absorption takes place in the blue part of the visible range and especially the near-UV interval.

The quantum-chemical calculations for Cp_2TiCl_2 [40] demonstrate the existence of three groups of electronic energy levels: (1) LOMO (lower lying occupied molecular orbitals) representing principally bonding combinations of the metal (M) and chloride ligand (X) atomic orbitals, (2) LUMO (lowest unoccupied molecular orbitals) which are mostly anti-bonding combinations of the same M and X orbitals, the lowest among them (denoted $2a_1$ below[1]) being composed almost completely by metal d-orbitals (M), (3) an intermediate group of orbitals, HOMO (highest occupied MO) of different symmetries ($1a_1$, $1a_2$, $1b_1$, $1b_2$), the latter having the highest energy. They represent bonding combinations of M and Cp orbitals (except for $1b_1$ which is Cp–M nonbonding), with a small contribution of anti-bonding combinations of M and X atomic orbitals. The highest among them is orbital $1b_2$. All 16 valence electrons of this complex in the Ti(IV) oxidation state are distributed among the LOMO and HOMO orbitals, and there are no partially occupied levels. Therefore, the observed absorption bands of this complex are interpreted as the lowest among the distances between these electronic levels, with restrictions imposed by the symmetry: $1b_2 \rightarrow 2a_1$, $1b_1 \rightarrow 2a_1$, $1a_1 \rightarrow 2a_1$ (transition $1a_2 \rightarrow 2a_1$ is symmetry forbidden). The first two of these transitions correspond predominantly to the transfer of the electronic density from the Cp ligands to the metal, i.e., ligand-to-metal (Cp→M) charge-transfer bands. Thus, obtained electronically excited singlet state is subject to a rapid transition to the corresponding lower-lying triplet state which (at low temperatures) possesses a very long lifetime and whose transition to the ground state is accompanied by the phosphorescence [41, 42]. The transition with the lowest excitation energy, $1b_2 \rightarrow 2a_1$, diminishes the occupation of the Cp–M bonding orbital, $1b_2$, resulting in the weakening of the Cp–M bond which manifests itself experimentally by the photochemically induced dissociation of this ligand.

In view of the similarities in the electronic structure of the Ta(V) and Ti(IV) complexes and their spectral properties, one may expect that the above description for Cp_2TiCl_2 may also be valid, at least qualitatively, for the oxidized form of the tantalocene dichloride complex.

An equally detailed quantum-chemical theory is not available for the reduced states of the above complexes, i.e., those of Ta(IV) or Ti(III). The structure of one of such complexes (with two pentamethylated ligands), Cp^*_2TiX, $Cp^*=C_5Me_5$, for a series of ligands X was established in [43] with the use of EPR data and the general theory of the orbitals in bent metallocenes [39]. The complex of Ti(III) has an extra electron with respect to that of Ti(IV) so that the aforementioned occupied orbitals of Cp_2TiCl_2, LOMO and HOMO, rest fully occupied, while the extra electron is placed to the lowest one among the previously empty (LUMO) levels, $2a_1$. In the Ti(IV) complex, this level corresponded to the electronically excited state after the light absorption for the lowest energies. In the reduced complex of Ti(III), this level is semi-occupied (i.e., semi-empty) in the ground state of the system so that the transitions to this level from the lower ones are still possible. However, one may assume that a strong electrostatic repulsion between two electrons in this state will shift the corresponding excitation energies upward compared to those for the same Ti(IV) complex. As a result, the lowest-energy excitations for the reduced complex correspond to the electronic transition from this boundary orbital, $2a_1$, to upper-lying LUMO levels, $2a_1 \rightarrow 2b_2$, $2a_1 \rightarrow 2b_1$, $2a_1 \rightarrow 3a_1$ (transition $2a_1 \rightarrow 2a_2$ is symmetry-forbidden). As all these four involved states were originated principally from the atomic d-orbitals of the metal (with some contributions from π-orbitals of Cp), the energy of this electronic transitions are generally lower than those for the previous case, Ti(IV). According to experimental data [43] for electronic spectra of the series of Cp^*_2TiX complexes, the lowest-energy transition, $2a_1 \rightarrow 2b_2$, is even located in the IR range. The theoretical estimations for the energy of this transition for this series based on the EPR data (the value for Cp^*_2TiCl is 2,852 cm^{-1}, i.e., 3,510 nm) matches well to the corresponding experimental data for the complexes for which this band was possible to observe (above 5,000 cm^{-1}). Two other transitions, $2a_1 \rightarrow 2b_1$ and $2a_1 \rightarrow 3a_1$, correspond to the energies in the visible range, in particular 648 and 552 nm for Cp^*_2TiCl. Their peak separation is relatively small so that they form a single broad band responsible for the color of their solutions.

As one can see from the spectrum for the initial state of the tantalocene complex, $Cp^*(CpSiMe_3)TaCl_2$, in Fig. 5

[1] For the sake to simply the notations in this discussion, the numeration of orbitals in our paper is different compared to those in [40] or [43] in which the complex in a single oxidation state was considered, that of Ti(IV) or Ti(III), while our discussion includes orbitals for both oxidation states. As an example, our orbitals $1a_1$, $2a_1$, $3a_1$ correspond to $13a_1$, $14a_1$, $15a_1$ in [40], while no notation for $1a_1$ and $1a_1$, $2a_1$ for two others in [43]

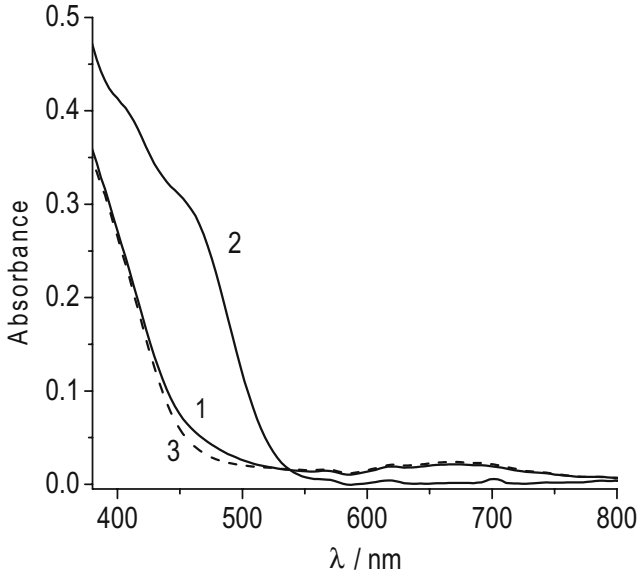

Fig. 5 Absorption spectrum of 15 mM Cp*($CpSiMe_3$)$TaCl_2$ + AN solution in the initial state before oxidation (neutral form) at polarization potential −0.62 V (curve 1) in the oxidized form at −0.42 V (curve 2) and again in the neutral form at −0.77 V after the end of reduction (curve 3)

(see also Fig. 6 below), there is a broad absorption band from about 600 to 750 nm which corresponds qualitatively to the observations for the analogous Ti(III) complex.

Kinetics of the spectral changes for redox transformation of Cp*$CpSiMe_3TaCl_2$ in acetonitrile solution

In the spectroelectrochemical experiments performed in the chronoamperometric regime, the electrode potential was stepped first from −0.62 to −0.42 V (corresponding to the oxidized state of the complex), and 300 consecutive absorption spectra were registered. The time of registration of each spectrum was 3 ms, time between spectra registration was 3 s. Then, the electrode was polarized by another step to −0.77 V (to induce the back transformation of the cationic complex into the initial neutral state), and again 300 subsequent spectra were recorded.

It is worth noting that after the end of this procedure (oxidation and reduction), the final spectrum returned to its initial state (cf. curves 1 and 3 in Fig. 5), in conformity with the reversible character of voltammograms (Figs. 2, 3 and 4) for this redox transition. Figure 5 presents also the spectrum for the end of the oxidation period (curve 2). The comparison of these spectra allows one to see the overall effect of the transformation of the complex from the neutral, Ta(IV), into the cationic, Ta(V), form.

The information of the kinetics of this process can be obtained from spectral curves measured in the course of this transformation. Figure 6 presents the initial and 1st, 2nd 3rd, 4th, 5th, 6th, 7th, 9th, 14th, and 300th spectra for oxidation (a) and the same sequence of spectra for reduction (b).

As visible from the data presented in Fig. 6a, oxidation of Cp*$CpSiMe_3TaCl_2$ results in gradual decrease of the absorption band at 670 nm, with simultaneous increase of absorption in the range below 535 nm where a shoulder is gradually formed at about 455–460 nm. A similar change of the spectrum (but in the opposite direction) takes place in the course of the complex reduction (Fig. 6b).

Kinetics of the transformation can be established from the analysis of the evolution of the difference spectra, e.g., those in Fig. 7a for oxidation of the complex obtained by subtraction of the initial spectrum.

First, one can note an isosbestic point at 535 nm for all curves (the same is valid for the reduction process), an indication that the changes in the spectra are due to transformation between two particular complexes, i.e., a single species for each oxidation state, Ta(IV) and Ta(V), in conformity with Eq. 1.

For a more quantitative treatment, the absorbance values (Fig. 6) at 445 and 670 nm, i.e., for both peaks in the

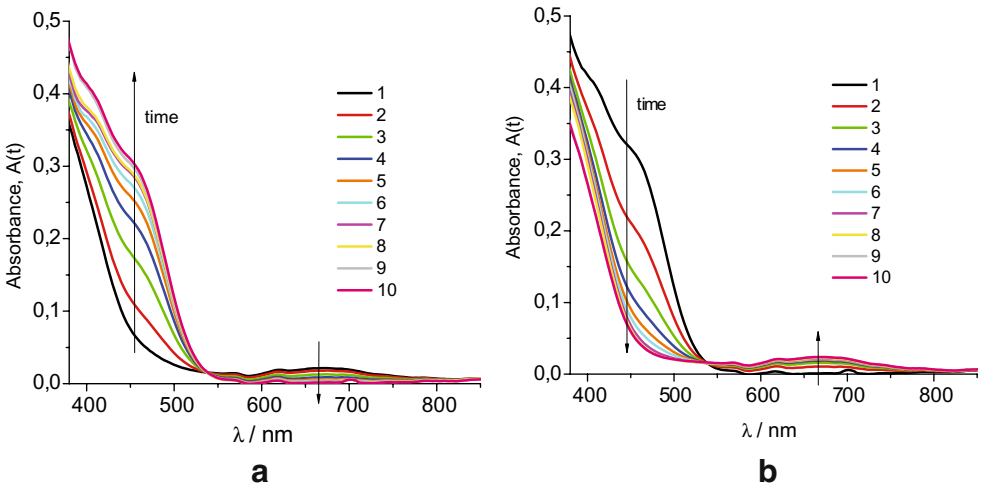

Fig. 6 Evolution of absorption spectrum of the solution of Cp*$CpSiMe_3TaCl_2$ in thin-layer spectroelectrochemical cell in response to the potential step applied to the electrode: initially from −0.62 to −0.42 V (**a**) then from −0.42 to −0.77 V (**b**). The spectra were collected after 0 (*1*), 3 (*2*), 6 (*3*), 9 (*4*), 12 (*5*), 15 (*6*), 18 (*7*), 24 (*8*), 39 (*9*), and 900 s (*10*) from the beginning of electrolysis. The changes of the spectrum are practically completed within 30–40 s after the potential step

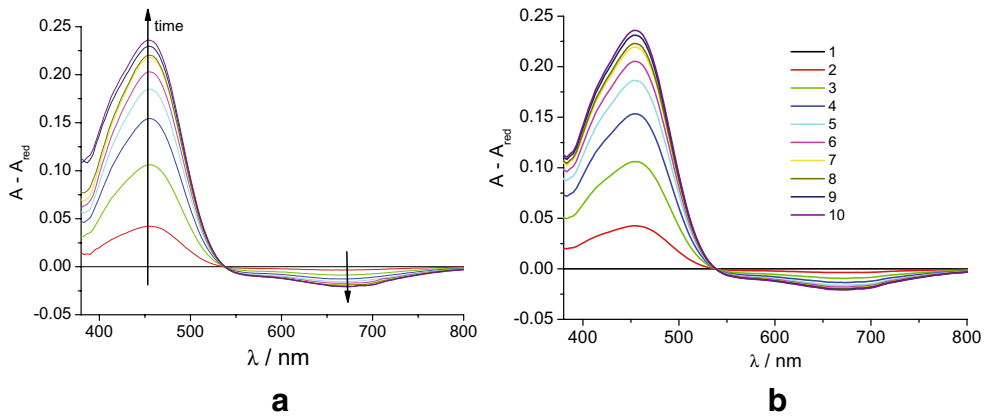

Fig. 7 **a** Changes of absorbance due to oxidation of Cp*CpSiMe$_3$TaCl$_2$ by the step of the electrode potential from −0.62 to −0.42 V. The plots, $\Delta A(t)=A(t)-A_{red}$, were obtained by subtraction of the initial spectrum (for the neutral complex), A_{red}, from the *n*th spectrum in Fig. 6a for oxidation of the complex, $A(t)$. **b** Simulated plots, $\Delta A(t)$ calculated on the basis of Eq. 15, i.e., by multiplication of the ΔA_{max} data for all wavelengths by a constant factor specific for each time moment: 0 (*1*), 0.18 (*2*), 0.45 (*3*), 0.65 (*4*), 0.79 (*5*), 0.87 (*6*), 0.93 (*7*), 0.945 (*8*), 0.98 (*9*), 1 (*10*)

difference spectra in Fig. 7a, were plotted as functions of time both for the oxidation and reduction processes. Then, these data were presented in the "normalized form" (Fig. 8) with the use of the formula:

$$\Delta A_{norm}(t) = (A(t) - A_{ox})/(A_{red} - A_{ox}) \quad (3)$$

where $A(t)$ is the absorbance at 455 or 670 nm for time t, A_{red} and A_{ox}, the limiting values of this quantity for completely reduced or oxidized state. In Fig. 8, the decreasing branches of the curves for both peaks characterize the oxidation process, while the increasing ones represent the evolution after the reduction step. For all these curves, the temporal coordinate, t, gives the time passed after the corresponding potential step.

An important observation in this figure is a practical coincidence of the normalized curves for two peaks, both in the course of the oxidation and of the reduction. It represents a further proof that each oxidation state of the complex, Ta(IV) and Ta(V), corresponds to a single molecular form.

The oxidation and reduction branches of the curve in Fig. 8 can be simulated by equations:

$$\Delta A_{\mathrm{norm}}(t) = \exp(-0.14t) \quad \text{for oxidation} \quad (4a)$$

$$\Delta A_{\mathrm{norm}}(t) = 1 - \exp(-0.18t) \quad \text{for reduction} \quad (4b)$$

Theory of thin-layer spectroelectrochemical response. Application to the data for the tantalocene derivative

Interpretation of these data is to be based on the theory of the thin-layer voltammetry for the time variation of the absorbance of the layer. It will be assumed that the transformation takes place between two forms (i.e., a single molecular form for each oxidation state), Ox and Red, and that the total amount of these species inside the layer remains constant, i.e., the exchange with the outer solution will be neglected.

As the absorbance at moment t, $A(t)$, is related to the total amounts (per unit surface area of the electrode) of the reduced and oxidized forms inside the solution layer, N_{red} and N_{ox} as well as their extinction coefficients, $\varepsilon_{\mathrm{red}}$ and $\varepsilon_{\mathrm{ox}}$:

$$A(t) = 2(N_{red}(t)\varepsilon_{red} + N_{ox}(t)\varepsilon_{ox}) \quad (5)$$

(coefficient 2 takes into account the passage of the beam through the layer two times), Eq. 3 for the normalized difference, $\Delta A_{\mathrm{norm}}(t)$, can be represented as:

$$\Delta A_{norm}(t) = N_{red}(t)/N_{red}^{\circ} \quad (6)$$

N_{red}° being the total amount of the complex in the layer (per unit surface area). Thus, the data in Fig. 8 show the evolution of the amount of the reduced form (with respect to its initial value, N_{red}°) which is related to its concentration inside the layer, $N_{red}(t) = \int_0^L c(x,t)dx$, L being the layer thickness.

In our experiments, the initial and final potential values for each step were chosen to realize the conditions of the limiting diffusion at the electrode surface. Therefore, the effects of a slow kinetics of the charge transfer will be disregarded.

Diffusion-limited transport (no ohmic effects)

Let us assume first that the effects of the ohmic resistance in the solution between WE and RE can be neglected. Then, the temporal variation in Fig. 8 may be interpreted on the basis of the conventional theory for the reactant

diffusion across the thin layer. The concentration profile, $c(x,t)$, obeys the non-stationary Fick equation with the initial and boundary conditions, e.g., for the oxidation process:

$$c(x,0) = c^{\circ},\ \ c(0,t) = 0,\ \ dc(x,t)/dx = 0\ \ for\, x = L \qquad (7)$$

c°, initial concentration of the complex, x=0 corresponds to the electrode surface, x=L, coordinate of the insulating surface (internal surface of the wall of the cell). Its solutions for the concentration distribution and for the fraction of the reduced form in the total amount inside the layer are given by formulas [44–47]:

$$c(x,t) = c^{\circ}\sum_{n=0}^{\infty} 2\lambda_n^{-1}\exp\left(-\lambda_n^2\, t\ D_{red}/L^2\right)\sin\lambda_n x/L,$$
$$N_{red}(t)/N_{red}{}^{\circ} = \sum_{n=0}^{\infty} 2\lambda_n^{-2}\exp\left(-\lambda_n^2\, t\ D_{red}/L^2\right),\ \ \lambda_n = \pi(n+0.5) \qquad (8)$$

where D_{red} is the diffusion coefficient of the reactant (reduced complex in our case). Except for a short time interval after the potential step, the variation of the latter quantity is given by the first term of the series:

$$N_{red}(t)/N_{red}{}^{\circ} \approx 8\pi^{-2}\exp\left(-0.25\pi^2\, t\ D_{red}/L^2\right),$$
$$8\pi^{-2} \approx 0.81,\quad 0.25\pi \approx 2.47 \qquad (9a)$$

For the reduction step, the same formulas are valid for the corresponding characteristics of the oxidized form (with the replacement of D_{red} by D_{ox}). As within the framework of the "thin-layer approximation" $N_{ox} + N_{red} = N_{red}{}^{\circ}$, Eq. 9a for the reduction period can be written as:

$$N_{red}(t)/N_{red}{}^{\circ} \approx 1 - 8\pi^{-2}\exp\left(-0.25\pi^2\, t\ D_{ox}/L^2\right), \qquad (9b)$$

Comparison of the exponential terms in Eqs. 9a and 9b [with the use of Eq. 6 for $A_{\mathrm{norm}}(t)$] with those in its empirical expressions 4a and 4b for the oxidation and reduction periods enabled us to determine the parameters of the system:

$$L^2/D_{red} \approx 17.6\ s,\quad L^2/D_{ox} \approx 13.7\ s \qquad (10)$$

The uncertainty in the exact value of the thickness of the solution layer in this measurement, L, did not allow us to establish the values of the diffusion coefficients, D_{red} and D_{ox}, from Eq. 10. The insertion of the expected range for the thickness, L=100–200 nm into Eq. 10 gives broad intervals for these parameters:

$$D_{red} = (0.57 - 2.3)10^{-5} cm^2/s;\quad D_{ox} = (0.73 - 2.9)10^{-5} cm^2/.s \qquad (11)$$

These crude estimates for the diffusion coefficients of the initial complex, Cp*(CpSiMe$_3$)TaCl$_2$, and of its oxidized (cationic) form can be compared with the data obtained for metallocene complexes of Ti as well as with the values estimated on the basis of the CV curves in Fig. 2.

The value of the diffusion coefficient of the non-substituted tantalocene complex, Cp_2TaCl_2, can be compared with that for an analogous titanocene complex, Cp_2TiCl_2, about 1.4–1.6×10^{-5} cm^2/s in AN obtained on the basis of CV data in the TEACl electrolyte (Vorotyntsev et al., unpublished data). The diffusion coefficients for the modified complex, Cp*(CpSiMe$_3$)TaCl$_2$, and its oxidized (cationic) form should be slightly lower. The effect of substitution in one of the Cp ligands can be seen from comparison of the values of D for Cp_2TiCl_2 and "titanocene–propyl–pyrrole" species, $(C_4H_4N(CH_2)_3C_5H_4)CpTiCl_2$, the latter value being about 0.9–1.0×10^{-5} cm^2/s.

Another estimate of the diffusion coefficient for the tantalocene complex, Cp*(CpSiMe$_3$)TaCl$_2$, can be obtained from the intensity of its oxidation wave in Fig. 2a, i_{pa}= 17.6–18.0 μA. It gives the value of about 1.0–1.05×10^{-5} cm^2/s which is in a satisfactory agreement with the values for the titanocene complexes as well as with the kinetic data in Eq. 10 if the solution layer thickness is 130–140 μm.

Taking into account that the value of the layer thickness L should be the same for the oxidation and reduction steps, Eq. 10 allows us to determine the ratio of the diffusion coefficients, $D_{\mathrm{ox}}/D_{\mathrm{red}}$. Then, the above estimate for D_{red} gives D_{ox}=1.3–1.35×10^{-5} cm^2/s.

Thus, obtained values for the diffusion coefficients of the complex in its neutral (reduced) and charged (oxidized) forms should only be considered as estimations, as neither its concentration for the data in Fig. 2a nor the thin-layer thickness, L, in Eq. 10 are known with a sufficient precision. On the contrary, the ratio of these diffusion coefficients seems to be determined more reliably: Assuming the thickness of the layer, L, to be the same for the oxidation and reduction stages, Eq. 10 gives an estimate for the ratio: $D_{\mathrm{ox}}/D_{\mathrm{red}}$≈1.25–1.3.

The found value is based on the simulation of the spectroelectrochemical data in Fig. 8 by Eqs. 4a, 4b and the model described in section "Diffusion-limited transport (no ohmic effects)". Their modification (e.g., to take into account the ohmic effects, see below) may influence both the values of the diffusion coefficients and their ratio. However, the conclusion on a noticeably higher rate of the diffusional transport for the oxidized form, compared to that for the reduced one, seems to be well established, as it is the only factor which may explain a definitely higher evolution of the spectral curve for the back (re-reduction) potential step, in conditions where the rates of the electrode processes for both steps were diffusionally controlled.

Both forms of the complex correspond to the same chemical structure, and the difference between them is in a higher charge of the central metal ion for the oxidized state,

Ta(V). One may suppose that this increase of the metal charge results in a stronger attraction force between this ion and the negatively charged ligands, Cp, Cp* and Cl, with a slight contraction of the complex (compared to its neutral/reduced state) leading to its higher transport rate.

Diffusion-limited transport with ohmic effects in the outer solution

The analysis in the preceding section has shown that the rate of the spectral changes matches qualitatively to the predictions of the conventional thin-layer theory, with the value of the diffusion coefficient corresponding well to the value found from the cyclic voltammetry. However, a more attentive analysis reveals an experimental indication to the need in elaborating this pure diffusional theory.

This theory predicts that the normalized total amount of the reactant inside the layer, $\Delta A_{norm}(t) = N_{red}(t)/N_{red}{}^{\circ}$, should drop quickly during the oxidation process from 1 for t=0 to about 0.8 to follow after it an exponential behavior given by Eq. 9a. Similar behavior is also predicted for 1 $-\Delta A_{\mathrm{norm}}(t)$ during the reduction process, see Eq. 9b. However, the treatment of experimental data in Fig. 8 in semi-logarithmic coordinates (Fig. 9) points to the absence of the expected variation within the short time interval. As a whole, these experimental data are described much better by exponential approximations 4a and 4b with a pre-exponential factor equal to 1, compared to Eqs. 9a and 9b with the factor equal to 0.81, see Fig. 9.

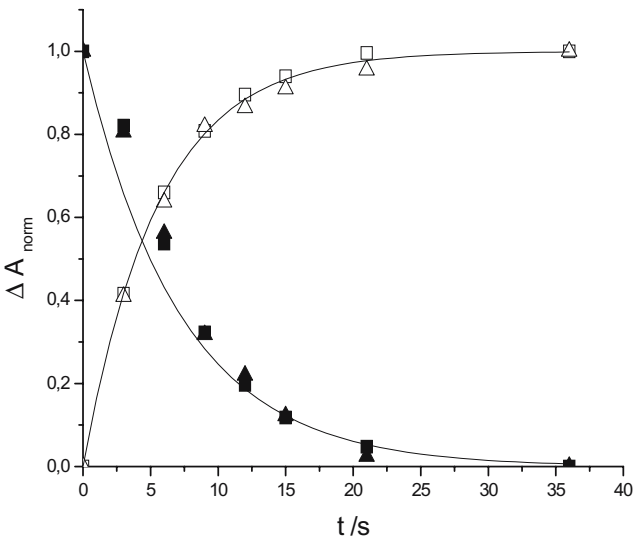

Fig. 8 Comparison of spectral changes for two characteristic wavelengths, 455 and 670 nm. The data for absorbance in Fig. 6 are presented as normalized changes of absorbance, ΔA_{norm} in Eq. 3, as functions of time for oxidation process (455 nm, *filled square*, and 670 nm, *filled triangle*) and for reduction process (455nm, *open square*, and 670 nm, *open triangle*). *X*-axis corresponds to the time passed after the corresponding (oxidation or reduction) potential step

This discrepancy may be related to significant ohmic potential differences which take place between RE (located in the bulk solution) and WE (inside the thin layer), in view of a very high electric resistance between the WE and RE in this geometry. Qualitative estimations of the latter parameter for the particular thin-layer cell used in our spectroelectrochemical experiments point to the possibility that this factor may affect the rate of the redox transformation between Ox and Red forms.

A quantitative treatment requires to generalize the theory of the diffusional transport inside a thin solution layer to take into account the distribution of the overall potential difference, E, between WE and RE into two contributions, the one at the WE/solution interface (which affects directly the kinetics of the redox transformation of the Ox or Red form) and the potential drop between the solution inside the thin layer and RE (which is proportional to the Faradaic current at WE and the electric resistance, R_{Ω}).

Mathematically, this problem is equivalent to that of the ion transport across a thin solid intercalation film at the electrode surface, with taking into account the "external" resistance (inside the solution and at the film/solution interface). The corresponding theory has been derived recently [45]; see also a further analysis in [48]. Then, the expression for the time variation of the normalized total amount of the reactant (e.g., for the oxidation step) can be obtained from the derived formulas for the non-stationary concentration profile:

$$\Delta A_{norm}(t) = N_{red}(t)/N_{red}{}^{\circ} = \Lambda\sum_{n=1}^{\infty} B_n\lambda_n^{-2}\exp\left(-\lambda_n^{-2}\, t\, D_{red}/L^2\right) \qquad (12)$$

where $\Lambda = R_d/R_{\Omega}, R_d = L^2/D_{red}C_{red}$ (C_{red} is total redox capacitance of the solution layer), R_{Ω} is electric resistance between the solution near the WE surface and RE, coefficients λ_{n} and B_{n} (n=1,2,...) are given by the formulas:

$$\lambda_n \tan\lambda_n = \Lambda\,(\text{transcendental equation}),$$

$$B_n = 2\Lambda\left(\Lambda^2 + \Lambda + \lambda_n^2\right)^{-1} \equiv 2\sin\lambda_n(2\lambda_n + 2\sin\lambda_n)^{-1}$$

In the limiting case of high values of parameter Λ ($R_{\Omega} \to 0$), Eq. 12 is reduced to Eq. 8 of the conventional theory, while the effect of the "external resistance" is noticeable for small or moderate values of this parameter.

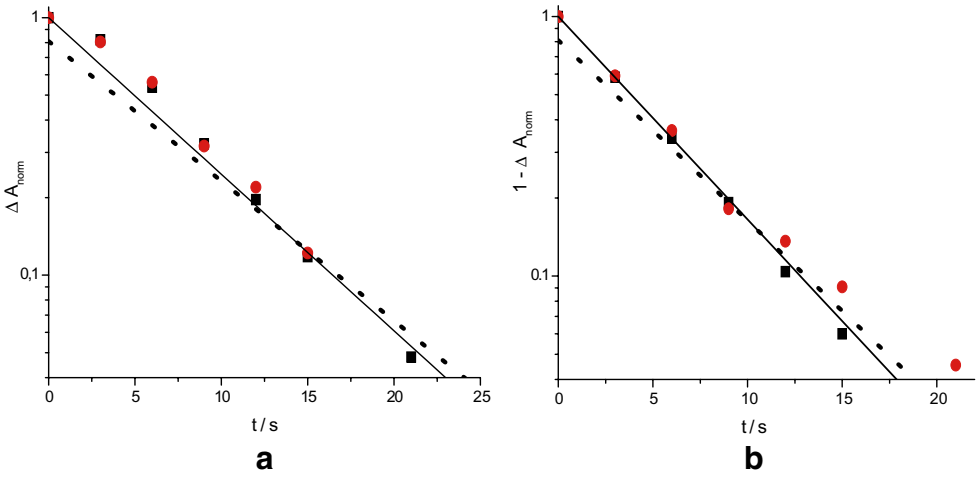

Fig. 9 Normalized spectral changes, $\Delta A_{norm}(t)$, as functions of time for oxidation (**a**, 455 nm, *filled square*, and 670 nm, *filled circle*) and for reduction (**b**, 455 nm *filled square*, and 670 nm, *filled circle*) steps, from Fig. 8, and their exponential fitting with the use of Eqs. 9a and 9b (*dotted lines*) and Eq. 13 (*solid lines*)

Similar to the previous case, in the most of the time interval (except a very short time range), the principal contribution to the sum is given by the first term of the sum so that

$$\Delta A_{norm}(t) = N_{red}(t)/N_{red}^{\circ} = K\exp\left(-\lambda_1^2 t\, D_{red}/L^2\right),$$

$$K = 2\Lambda^2\left(\Lambda^2 + \Lambda + \lambda_1^{-2}\right)^{-1}\lambda_1^{-2} \qquad (13)$$

Coefficient K in this formula is equal to 0.81 for high values of parameter Λ, i.e., for no ohmic potential drop, while λ_1 is close to $1/2\pi$ so that Eq. 13 is reduced to Eq. 8. In the opposite limiting case of a high resistance of the solution between WE and RE ($\Lambda \to 0$), K is close to 1, while $\lambda_1 \approx \Lambda^{1/2}$. A numerical analysis of general expression 13 shows that K approaches its limiting value, 1, rapidly: K= 0.96 for Λ=2, K=0.986 for Λ=1. It implies that even for these cases where the ohmic effects are still not strong, the linear plot in semi-logarithmic coordinates given by Eq. 13 should pass near the point (0; 1), in accordance with the experimental lines in Fig. 9.

One cannot determine the values of two unknown parameters, Λ and L, from a single value of the coefficient in the exponent of Eq. 4a or 4b, e.g., 0.14 s^{-1} for the oxidation. Therefore, one can only analyze whether one can satisfy simultaneously to both conditions that ΔA_{norm} has a value close to 1 for t=0 and that the plot, log ΔA_{norm} vs t, possesses a proper slope for the above found value of D_{red} and reasoning values of the solution layer thickness, L. The former condition is satisfied for the interval: $\Lambda \leq 2$. Then, the use of the numerical values of λ_1 allows us to obtain the estimates of the thickness, e.g.,: L=90–95 μm for Λ=2, which is in conformity with its expected range.

Analysis of global spectra changes

The above analysis was based solely on the time variation of the absorbance for two particular values of the light wavelength, λ. It cannot exclude a more complicated behavior at other wavelengths. For a more quantitative consideration, we have developed an alternative approach: The absorbance values for each graph in Fig. 7a (for the difference spectra) were divided by those at the end of the transformation (for the same wavelength).

It gives new plots for each time moment shown in Fig. 10. The points in the interval near 540 nm have been omitted, as the ratio of small values (in the vicinity of the isosbestic point in Fig. 6 corresponding to the zero in the difference spectra in Fig. 7a results in an irregular noise. For the rest of the whole interval of wavelengths above 440 nm, the plots are practically horizontal; in particular, the values for each plot above and below 540 nm are the same. It means that all curves in the difference spectra (Fig. 7a) can be represented as

$$\Delta A(t) \equiv A(t) - A_{red} = 2N_{ox}(t)(\varepsilon_{ox}(\lambda) - \varepsilon_{red}(\lambda)) \qquad (14)$$

with the same coefficient, $N_{ox}(t)$, for all wavelengths λ. It results in the formula:

$$\Delta A(t)/\Delta A_{max} = \text{function}\,(t) \quad \text{for all wave lengths} \qquad (15)$$

where the right-hand side is independent of the wavelength and equal to $N_{ox}(t)/N_{red}^{\circ}$, $\Delta A_{max} = A_{red} - A_{ox}$ in Eq. 3,

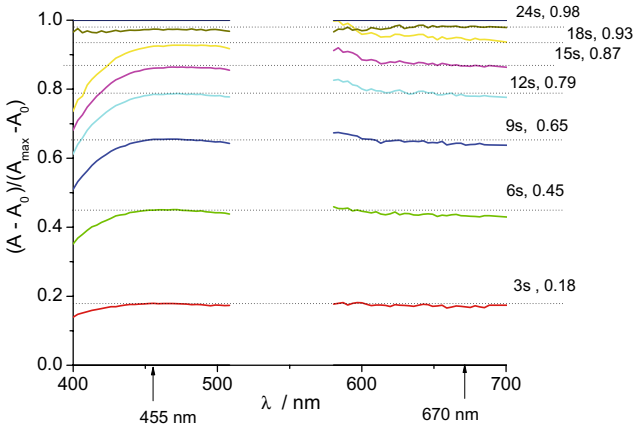

Fig. 10 Ratio of the difference spectra in Fig. 7a to the difference spectrum for the complete redox transformation of the complex

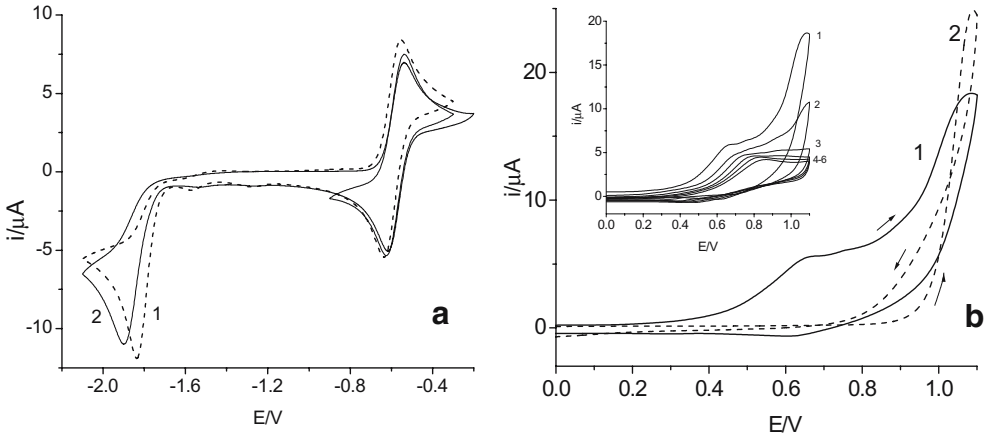

Fig. 11 **a** Comparison of cyclic voltammograms of $Cp^*CpSiMe_3$, $TaCl_2$ (curve 1) and $Cp^*(Cp(CH_2)_3Py)TaCl_2$ (curve 2) in AN containing 0.1 M $TBAPF_6$ in the potential range −0.9 V→−0.2 V→−2.1 V→−0.9 V. **b** Comparison of the first cyclic voltammograms obtained in 0.1 M $TBAPF_6$ + AN containing 3 mM $Cp^*(Cp(CH_2)_3Py)TaCl_2$ (curve 1) or 3 mM pyrrole (curve 2). *Inset* Consecutive scans in $Cp^*(Cp(CH_2)_3Py)TaCl_2$

change of the absorbance (at a certain wavelength) for a complete transformation of Ta(IV) to Ta(V).

All this analysis based on formula 5 is only valid if the absorption is always due to *two* species with a constant total amount, $N_{red}°$. The appearance of other products would lead to the violation of the constancy of plots in Fig. 9 in the range where the absorption properties of different final species are not identical. In this context, one may pay attention to the range below 440 nm where a deviation is observed, but this range of wavelengths is already close to the limit of the measurement device.

According to Eq. 15, the value of the ratio (which should be independent of the wavelength) determines the degree of transformation of Ta(IV) to Ta(V) form. These values (indicated at each plot in Fig. 9) were multiplied by the difference spectrum for the complete transformation, $\Delta A_{max}(\lambda)$, to obtain the simulated difference spectra in Fig. 7b. The comparison of simulated and experimental plots in Fig. 7a,b shows a very close proximity of the corresponding curves, except for the lowest wavelength range. Thus, one may deduce the final conclusion on a single product of the complex oxidation, which is in conformity with electrochemical evidences, Eq. 1.

Electrochemical behavior and polymerization of $Cp^*(Cp(CH_2)_3Py)TaCl_2$ (**2**) on Pt electrode

Another organometallic complex of Ta studied in this paper also contains Cp* and two chloride ligands, while the fourth ligand was changed from Cp or $CpSiMe_3$ (in **1**) to $Cp(CH_2)_3Py$ (in **2**) linked to pyrrole (Py) group via nitrogen. One could expect a similarity of redox properties of these complexes related to oxidation or reduction of Ta, while the presence of Py group opened the prospect of its electropolymerization to obtain a conducting polymer film with the polypyrrole matrix and attached tantalocene dichloride complexes, as in the case of titanocene dichloride studied by us earlier [24, 25].

In conformity with the former expectation, the redox behavior of $Cp^*(Cp(CH_2)_3Py)TaCl_2$ on Pt electrode in acetonitrile solution in the potential range between −0.3 and −2.1 V is nearly the same as that observed for compound **1** (Fig. 11a). For both complexes, the redox peaks of reversible tantalum transformation are located at about the same potentials, while the peak of irreversible reduction for the complex containing $Cp(CH_2)_3Py$ ligand is slightly shifted (by about 70 mV) towards more negative potentials,

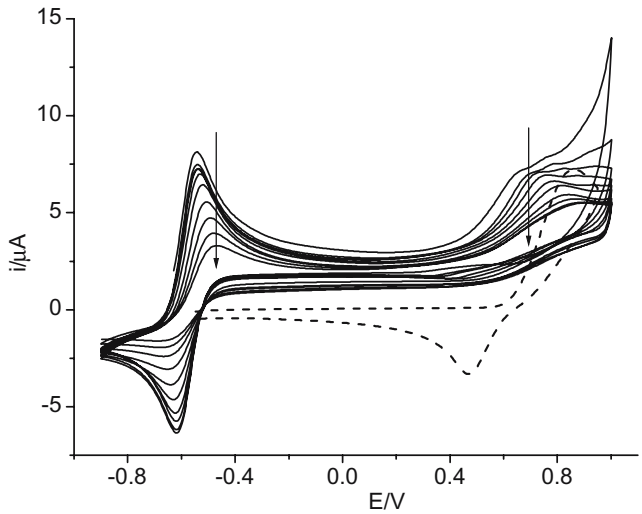

Fig. 12 Cyclic voltammograms (ten consecutive scans) for Pt electrode in the solution of 3 mM $Cp^*(Cp(CH_2)_3Py)TaCl_2$ + 0.1 M $TBAPF_6$/AN at the scan rate of 100 mV/s. *Dashed line* corresponds to the CV on Pt electrode in the solution of 2 mM TEACl/AN (without monomer)

see Table 1. The voltammogram is stable in the course of consecutive cycling provided that the solution is free of oxygen.

In the first cycle performed in the solution of Cp*(Cp$(CH_2)_3$Py)$TaCl_2$ in the range from 0 to 1.1 V, there is an anodic wave at about 0.7 V followed by the current peak at 1.08 V (curve 1 in Fig. 11b). A comparison with the cyclic voltammogram of pyrrole (curve 2) indicates that the anodic maximum at 1.08 V results from oxidation of the pyrrole ring in the complex. However, the consecutive cyclic voltammograms carried out in Cp*(Cp$(CH_2)_3$Py)$TaCl_2$ solution (Fig. 11b, inset) do not show the formation of an electroactive polymer film on the electrode. The current of the monomer oxidation strongly decreases in the second cycle; the first wave shifts to more positive potentials, and no cathodic wave characteristic of polymer reduction is seen. These observations testify in favor of the electrode surface blocking by a very thin insulating film.

To check whether this inhibition of the surface might originate from the first layer of the deposited polymer overoxidized due to too high anodic potentials, the polymerization procedure was repeated for a lower anodic limit of the potential scan. However, the same behavior was observed when the range of positive potentials was limited to 1 V, while the negative one was extended to −0.9 V to control also the changes in the range of redox transformation of Ta (Fig. 12).

In the first cycle, one can see the same anodic waves as well as a pair of reversible redox peaks around −0.6 V already discussed in section "Electrochemical behavior of Cp*CpSi$Me_3$$TaCl_2$ and Cp*Cp$TaCl_2$ in AN and THF solutions" and related to the transformation of the tantalocene complex. The subsequent scans lead to gradual decrease of all oxidation and reduction waves, which is typical for formation of a highly resistive layer on the electrode.

A quite similar behavior was observed during polymerization of pyrrole and titanocene-pyrrole derivative in the presence in solution of small amounts of chloride anion [49]. Oxidation of Cl^- ions in sufficiently dry AN solutions starts in the same potential range as monomer oxidation (see dashed line in Fig. 12). In effect, product of chloride oxidation or Cl^- ions itself cause chlorination of the monomer or radical cation and/or react with already deposited polymer, leading to decrease of its electroactivity and electric conductivity. As one can see from the description of the monomer synthesis (Synthesis of tantalocene complexes), the monomer used in this study, Cp*(Cp$(CH_2)_3$Py)$TaCl_2$, contained chloride ions after its synthesis on the basis of Cp*$TaCl_4$. In analogy with previous unsuccessful attempts of the polymer deposition [49], the presence of chloride anions in dry AN solution of a monomer results in an earlier onset and a higher intensity of the oxidation current (compared to those of both the chloride itself or the monomer in the chloride-free solution), with a shoulder before the principal oxidation wave, in conformity with voltammograms in Fig. 11.

Conclusions

Our voltammetric study of tantalocene dichloride complexes, Cp*(Cp-R)Ta(IV)Cl_2, with three different groups R: H, $SiMe_3$ or $(CH_2)_3NC_4H_4$, has shown a close similarity of their redox responses to that of the non-substituted complex, Cp_2TaCl_2: a reversible transformation for the oxidation process, Ta(IV)/Ta(V), while an irreversible response for the reduction process, Ta(IV)/Ta(III), because of a rapid loss of one of the chloride ligands after the electron transfer.

The former transition in the Cp*(Cp$SiMe_3$)Ta(IV)Cl_2 complex has also been studied by the spectroelectrochemical technique inside a thin AN solution layer. It allowed us to measure the UV-visible absorption curves for the initial and oxidized states, Ta(IV) and Ta(V), as well as to trace the evolution of this spectrum from the reduced (initial) to the oxidized state and back. Analysis of this kinetic changes and of the voltammetric data for this complex has led to the conclusion that each of these oxidation states of this complex are presented by a single molecular form. The diffusion coefficients for this complex in both reduced and oxidized states have been evaluated.

Oxidation of the pyrrole-containing complex, Cp*(Cp$(CH_2)_3NC_4H_4$)Ta(IV)Cl_2, results in the formation of a thin insulating film at the electrode surface which inhibits the oxidation processes both of the tantalum complex and of the pyrrole ring, thus, preventing the growth of a conducting polymer film. This result has been attributed to an effect of chloride anions (present in the complex because of the synthesis procedure) which transform pyrrole oligomers and the deposited conjugated polymer molecules into chlorinated species, similar to our previous observations for polypyrrole and its derivatives.

Acknowledgements MS expresses a gratitude to the University of Bourgogne for her invitation as invited professor. We are also thankful to Herman John for the help during spectroelectrochemical experiments.

References

1. Molander GA, Harris CR (1996) Chem Rev 96:307
2. Gansauer A (1997) Synlett 4:363
3. Skrydstrup T (1997) Angew Chem Int Ed Engl 36:345
4. Molander GA, Harris CR (1998) Tetrahedron 54:3321
5. Krief A, Laval AM (1999) Chem Rev 99:745
6. Gansauer A, Bluhm H, (2000) Chem Rev 100:2771

7. Spencer RP, Schwartz J, (2000) Tetrahedron 56:2103
8. Gansauer A (2001) In: Renaud P, Sibi MP (eds) Radicals in organic synthesis. Wiley-VCH, Weinheim, Germany, p 2007
9. Li JJ (2001) Tetrahedron 57:10
10. Steel PG (2001) J Chem Soc Perkin Trans 1:2727
11. Wolczanski PT, Bercaw JE (1982) Act Chem Rex I3:21
12. Thompson ME, Bercaw JE (1984) Pure Appt Chem 56:1
13. Hillhouse GL, Bercaw JE (1985) J Am Chem Soc 106:5474
14. Doherty NM, Bercaw JE (1985) J Am Chem Soc 107:2670
15. Bell RA, Cohen SA, Doherty NM, Threlkel RS, Bercaw JE (1986) Organometallics 5:972
16. Schottenberger H, Reussner J, Buchmeiser M, Neissl W, Elsner O, Angleitner H, Ernst E (1995) Eur Pat Appl 21
17. Feng S, Roof GR, Chen EY-X (2002) Organometallics 21:832
18. Mariott WR, Gustafson LO, Chen EY-X (2006) Organometallics 25:3721
19. Mariott WR, Hayden LM, Chen EY-X (2003) ACS Symposium Series 857:101
20. Foust DF, Rogers RD, Rausch MD, Atwood JL (1982) J Am Chem Soc 104:5646
21. Curtis MD, Bell LG, Butler WM (1985) Organometallics 4:701
22. Hunter JA, Lindsell WE, Mc Cullough KJ, Parr RA, Scholes ML (1990) J Chem Soc Dalton Trans 2145
23. Kukharenko SV, Soloveichik GL, Strelets VV (1990) Metalloorganicheskaya Khimiya 3:88
24. Vorotyntsev MA, Casalta MM, Pousson E, Roullier L, Boni G, Moise C (2001) Electrochim Acta 46:4017
25. Vorotyntsev MA, Skompska M, Pousson E, Goux J, Moise C (2003) J Electroanal Chem 552:307
26. Skompska M, Vorotyntsev MA, Refczynska M, Goux J, Lesniewska E, Boni G, Moise C (2006) Electrochim Acta 51:2108
27. Vorotyntsev MA, Graczyk M, Lisowska-Oleksiak A, Goux J, Moise C (2004) J Solid State Electrochem 8:818
28. Magdesieva TV, Nikitin OM, Demyanov PI, Graczyk M, Vallat A, Vorotyntsev MA, Butin KP (2005) Rus Chem Bull Intern Ed 54:201
29. Magdesieva TV, Graczyk M, Vallat A, Nikitin OM, Demyanov PI, Butin KP, Vorotyntsev MA (2006) Electrochim Acta 52:1265
30. Gibson VC, Bercaw JE, Bruton WJ, Sanner RD (1986) Organometallics 5:976
31. Castro A, Gómez M, Gómez-Sal P, Manzanero A, Royo P (1996) J Organomet Chem 518:37
32. Goux J, Le Gendre P, Richard P, Moïse C (2005) Organometallics 24:4902
33. Geskes C, Heinze J (1996) J Electroanal Chem 418:167
34. Broussier R, Bourdon C, Blacque O, Vallat A, Kubicki MM, Gautheron B (1997) J Organomet Chem 538:83
35. Mugnier Y, Fakhr A, Fauconet M, Moise C, Laviron E (1983) Acta Chem Scand B37:423
36. Goux J, Le Gendre P, Richard P, Moise C (2006) J Organometal Chem 691:3239
37. Mugnier Y, Moise C, Laviron E (1981) J Organomet Chem 204:61
38. Mugnier Y, Moise C, Laviron E (1981) J Organomet Chem 210:69
39. Lauher JW, Hoffmann R (1976) J Am Chem Soc 98:1729
40. Bruce MRM, Kentner A, Tyler DR (1984) J Am Chem Soc 106:639
41. Kenney JW, Boone DR, Striplin DR, Chen YH, Hamar KB (1993) Organometallics 12:3671
42. Loukova GV, Smirnov VA (2000) Chem Phys Lett 329:437
43. Lukens WW, Milton RS, Andersen RA (1996) J Am Chem Soc 118:1719
44. Wen CJ, Boukamp BA, Huggins RA, Weppner W (1979) J Electrochem Soc 126:2258
45. Montella C (2002) J Electroanal Chem 518:61
46. Diard JP, Le Gorrec B, Montella C (2001) J Electroanal Chem 499:67
47. Levi MD, Aurbach D (1999) Electrochimica Acta 45:167
48. Vorotyntsev MA, Levi MD, Aurbach D (2004) J Electroanal Chem 527:299
49. Skompska M, Vorotyntsev MA (2004) J Solid State Electrochem 8:360